Role of persistent sodium current in mouse preBötzinger Complex neurons and respiratory rhythm generation

Ryland W. Pace[1], Devin D. Mackay[2], Jack L. Feldman[2] and Christopher A. Del Negro[1,2]

[1]*Department of Applied Science, The College of William and Mary, Williamsburg, VA 23187-8795, USA*
[2]*Systems Neurobiology Laboratory, Department of Neurobiology, David Geffen School of Medicine at the University of California Los Angeles, Box 951763, Los Angeles, CA 90095-1763, USA*

Breathing movements in mammals depend on respiratory neurons in the preBötzinger Complex (preBötC), which comprise a rhythmic network and generate robust bursts that form the basis for inspiration. Persistent Na^+ current (I_{NaP}) is widespread in the preBötC and is hypothesized to play a critical role in rhythm generation because of its subthreshold activation and slow inactivation properties that putatively promote long-lasting burst depolarizations. In neonatal mouse slice preparations that retain the preBötC and generate a respiratory-related rhythm, we tested the role of I_{NaP} with multiple Na^+ channel antagonists: tetrodotoxin (TTX; 20 nM), riluzole (RIL; 10 μM), and the intracellular Na^+ channel antagonist QX-314 (2 mM). Here we show that I_{NaP} promotes intraburst spiking in preBötC neurons but surprisingly does not contribute to the depolarization that underlies inspiratory bursts, i.e. the inspiratory drive potential. Local microinjection in the preBötC of 10 μM RIL or 20 nM TTX does not perturb respiratory frequency, even in the presence of bath-applied 100 μM flufenamic acid (FFA), which attenuates a Ca^{2+}-activated non-specific cation current (I_{CAN}) that may also have burst-generating functionality. These data contradict the hypothesis that I_{NaP} in preBötC neurons is obligatory for rhythmogenesis. However, in the presence of FFA, local microinjection of 10 μM RIL in the raphe obscurus causes rhythm cessation, which suggests that I_{NaP} regulates the excitability of neurons outside the preBötC, including serotonergic raphe neurons that project to, and help maintain, rhythmic preBötC function.

(Received 8 November 2006; accepted after revision 31 January 2007; first published online 1 February 2007)
Corresponding author C. A. Del Negro: Department of Applied Science, McGlothlin-Street Hall, Room 303, The College of William and Mary, Williamsburg, VA 23187-8795, USA. Email: cadeln@wm.edu

Mammalian breathing depends on neurons in the preBötC that burst during inspiration. The network of preBötC neurons retains its rhythmic function in reduced *in vitro* and *in situ* preparations (Suzue, 1984; Smith *et al.* 1990, 1991; Paton, 1996), allowing the cellular and synaptic bases of respiratory rhythm generation to be examined within the context of inspiratory-related motor output via cranial and spinal motor nerves, notably the hypoglossal (XII) nerve.

Shortly after discovering that rhythmogenesis *in vitro* was independent of reciprocal postsynaptic inhibition (Feldman & Smith, 1989), neurons with voltage-dependent bursting-pacemaker properties were characterized in the preBötC (Smith *et al.* 1991; Johnson *et al.* 1994), which were subsequently shown to depend on persistent Na^+ current (I_{NaP}) (Del Negro *et al.* 2002*a*,*b*). These observations led to the hypotheses that I_{NaP} plays a key role in respiratory rhythm generation by: (i) giving rise to an obligatory subpopulation of rhythmically active *pacemaker* neurons, and; (ii) amplifying excitatory synaptic input in non-pacemaker neurons to promote robust inspiratory bursts throughout the preBötC network (Onimaru *et al.* 1995; Rekling & Feldman, 1998; Butera *et al.* 1999*b*, 2005; Smith *et al.* 2000; Ramirez *et al.* 2004; Feldman & Del Negro, 2006). Here, we address these hypotheses and conclude that pacemaker neurons are not obligatory for respiratory rhythm generation and I_{NaP} does not amplify synaptic inputs but it does enhance spike frequency.

The biophysical properties of I_{NaP} have been studied in synaptically isolated and dissociated preBötC neurons but not in the context of respiratory network function. At postnatal days (P) from P0–15, 5–15% of all preBötC neurons exhibit I_{NaP}-mediated bursting-pacemaker activity after synaptic isolation using a cocktail of receptor antagonists (Pena *et al.* 2004; Del Negro *et al.* 2005). The I_{NaP} bursting mechanism is now well understood (Butera *et al.* 1999*a*; Thoby-Brisson & Ramirez, 2001; Del Negro *et al.* 2002*a*; Ramirez *et al.* 2004). Nevertheless, all inspiratory neurons express I_{NaP} (Del Negro *et al.*

 DOI: 10.1113/jphysiol.2006.124602

2002*b*; Ptak *et al.* 2005) and receive rhythmic synaptic excitation when synaptic transmission and network function are intact (Funk *et al.* 1993). This led to the hypothesis that I_{NaP} amplifies synaptic excitation, which putatively augments inspiratory bursts throughout the preBötC during respiratory rhythm generation (Butera *et al.* 1999*b*; Smith *et al.* 2000; Del Negro *et al.* 2001, 2002*a*), which we test here.

The obligatory rhythmogenic role of pacemaker neurons and I_{NaP} in general is questionable because bath application of the Na^+ channel antagonist riluzole (RIL) rapidly blocks I_{NaP} and pacemaker activity at low doses (IC_{50} ~3 μM) but does not rapidly perturb the frequency of respiratory rhythms *in vitro* and *in situ* at doses much greater than 3 μM (Del Negro *et al.* 2002*b*, 2005; Paton *et al.* 2006). However, in addition to blocking I_{NaP}, RIL depresses excitatory transmission (Doble, 1996; Wang *et al.* 2004) and long duration, bath application of RIL causes the XII motor discharge to decline in amplitude (Del Negro *et al.* 2005).

In full recognition of the pharmacological caveats associated with blocking I_{NaP}, we present specific and relevant tests of its role in rhythm generation. First, we tested the role of I_{NaP} in synaptic amplification with an intact network. We employed intracellular QX-314 (2 mM) to block Na^+ currents in single neurons and measured changes in the *inspiratory drive potential*. We also bath-applied RIL (10 μM) and low doses of tetrodotoxin (TTX, 20 nM) to measure the contribution of I_{NaP} to inspiratory drive potential generation and intraburst spiking.

Second, we tested whether pacemaker neurons were required for rhythm generation by microinjecting RIL and TTX directly into the preBötC. We performed this experiment in the presence and absence of flufenamic acid (FFA, 100 μM); we did this because FFA blocks a Ca^{2+}-activated non-specific cation current (I_{CAN}), which engenders another class of bursting activity in neonates older than P8 (Thoby-Brisson & Ramirez, 2001; Ramirez *et al.* 2004). This drug-microinjection protocol blocks I_{NaP} locally within the preBötC and minimizes effects on I_{NaP} in neurons outside of the preBötC, such as XII motoneurons and serotonergic neurons in the raphe that may be critical for rhythm generation *in vitro* (Pena & Ramirez, 2002; Tryba *et al.* 2006) and perinatal breathing in infants (Paterson *et al.* 2006).

Here we show that I_{NaP} promotes spiking during inspiratory bursts but does not notably amplify synaptic excitation nor contribute to the underlying inspiratory drive potential. Also, blocking I_{NaP} in the preBötC does not stop rhythmogenesis even after attenuating I_{CAN}. We conclude that I_{NaP} in preBötC neurons is not critical for respiratory rhythm generation *in vitro*. However, our results suggest that I_{NaP} plays a role in respiratory-related neurons outside the preBötC that ultimately helps to maintain the general level of excitability in the preBötC to ensure rhythmogenesis.

Methods

We used neonatal C57BL/6 mice (P0–4) for experiments *in vitro*. The Office for the Protection of Research Subjects (University of California Animal Research Committee) and the Institutional Animal Care and Use Committee (The College of William and Mary) approved all protocols.

Neonatal mice were anaesthetized by hypothermia and rapidly decerebrated prior to dissection in normal artificial cerebrospinal fluid (ACSF) containing (mM): 124 NaCl, 3 KCl, 1.5 $CaCl_2$, 1 $MgSO_4$, 25 $NaHCO_3$, 0.5 NaH_2PO_4, and 30 D-glucose, equilibrated with 95% O_2 and 5% CO_2 with pH = 7.4. Transverse slices (550 μm thick) containing the preBötC, XII motoneurons and the raphe obscurus (Fig. 1*A*) were sectioned using a vibrating microslicer. The rostral cut was positioned just rostral

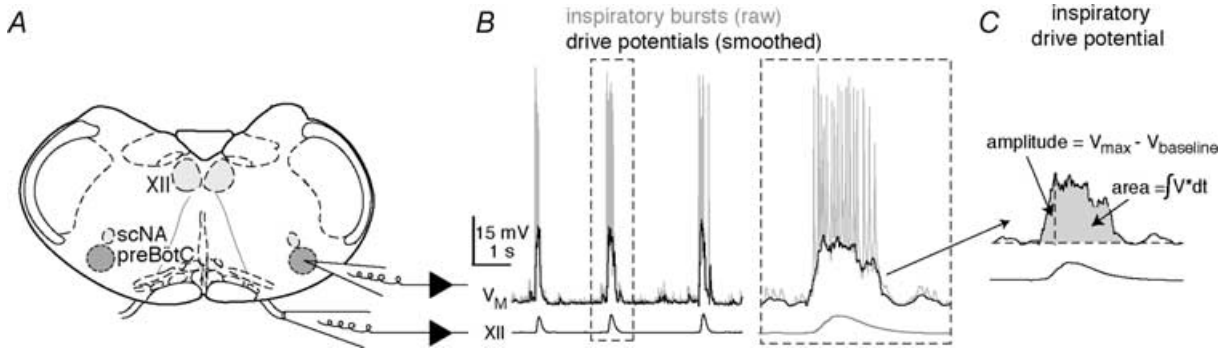

Figure 1. The *in vitro* slice preparation and experimental methodology
A, schematic depiction of the transverse slice preparation, illustrating bilateral preBötC and XII motor nuclei (XII), as well as the semicompact division of the nucleus ambiguous (scNA). Patch and suction electrodes are also illustrated. *B*, raw (grey) and smoothed (black) recordings of a preBötC neuron (V_M) and XII motor output. Dashed lines surround a burst that was plotted on an expanded time scale. *C*, the expanded burst from *B* (smoothed) is measured with regard to amplitude ($V_{max} - V_{baseline}$) and area ($\int V \times dt$) of the inspiratory drive potential.

to the rostral-most XII nerve roots at the level of the dorsomedial cell column and principal lateral loop of the inferior olivary nucleus, thus the preBötC was at or near the rostral surface (Ruangkittisakul *et al.* 2006). The caudal cut captured the obex. Slices were placed rostral surface up in a 0.5 ml recording chamber on a fixed-stage microscope equipped with Koehler illumination and perfused with 27°C ACSF at 4 ml min^{-1}. ACSF K^+ concentration was raised to 9 mM and respiratory motor output was recorded from XII nerve roots using suction electrodes and a differential amplifier (Fig. 1). In voltage-clamp experiments, $CaCl_2$ was reduced to 0.5 mM and replaced with equimolar $MgSO_4$ in order to block synaptic transmission and Ca^{2+} currents.

All electrical recordings were performed on inspiratory preBötC neurons, visually identified ventral to the semicompact division of the nucleus ambiguous (Fig. 1*A*), which exhibited an inspiratory discharge pattern (Fig. 1*B*). Since we focused on all inspiratory preBötC neurons, we did not attempt to identify neurons with pacemaker properties. Current-clamp recordings were performed using a Dagan IX2-700 amplifier (Minneapolis, MN, USA). Access resistance was compensated with bridge balance. Voltage-clamp recordings were performed using a HEKA EPC-10 amplifier (Lambrecht, Germany). Data were digitally acquired at 4–20 kHz using a 16-bit A/D converter after low pass filtering at 1 kHz to avoid aliasing. Additionally, access resistance was partially compensated with analog feedback. Intracellular pipettes were fabricated from capillary glass (o.d., 1.5 mm; i.d., 0.87 mm) and filled with one of two patch solutions.

The standard potassium gluconate patch solution contained (mM): 140 potassium gluconate, 5 NaCl, 1 EGTA, 10 Hepes, 2 Mg-ATP, and 0.3 Na-GTP (pH = 7.3 by KOH). In potassium gluconate experiments, pipette resistance was 3–4 MΩ and a liquid junction potential of 8 mV was corrected offline. In some cases, 2 mM QX-314, obtained from Sigma (St Louis, MO, USA), was added to the potassium gluconate patch solution in order to block Na^+ channels intracellularly. In these experiments, we obtained control measurements using nystatin-perforated patches. Nystatin (250 μg ml^{-1}) was added to the QX-314 patch solution immediately prior to use and was discarded after 120 min.

To analyse miniature synaptic potentials (e.g. Fig. 3), we used a Cs^+-based patch solution containing (mM): 110 CsCl, 20 TEA-Cl, 10 NaCl, 1.5 EGTA, 10 Hepes, 0.5 $CaCl_2.2H_2O$, 2 Mg-ATP, and 0.3 Na-GTP (pH = 7.3 by CsOH). In experiments using the Cs^+-based patch solution, pipette resistance was 3–4 MΩ and a liquid junction potential of 3 mV was corrected offline.

We either locally or bath-applied these drugs obtained from Sigma: FFA, RIL, muscimol (MUS), picrotoxin (PTX) and strychnine (STR). We obtained TTX from EMD Biosciences (San Diego, CA, USA). We used a micropressure ejection system (Toohey, Fairfield, NJ, USA) gated by an external transistor–transistor logic (TTL) pulse generator to deliver 8 ms-long drug applications at 3 Hz (8–12 p.s.i.). Microinjection pipettes with 8–15 μm tip diameter were fabricated from capillary glass and filled with 9 mM [K^+] ACSF containing MUS (15 μM), RIL (10 μM), or TTX (20 nM or 1 μM). During the microinjection protocols, the pipettes were placed either on (for the control MUS microinjections) or 100 μm below (for the TTX and RIL microinjections) the surface of the tissue. Before every microinjection experiment of RIL or TTX into the preBötC, bilateral MUS microinjections were first used to verify the location of the pipettes. Afterwards, the MUS injection protocol was stopped and slices were perfused with 9 mM [K^+] ACSF for > 15–20 min to wash out the effects of MUS before microinjecting RIL or TTX (Figs 5 and 6, and see Brockhaus & Ballanyi, 1998). RIL was bilaterally injected into the preBötC for > 40 min and 100 μM FFA was bath-applied for the last 20 min (Fig. 6*A*). TTX (20 nM) was bilaterally microinjected for > 10 min (Fig. 6*B*). In Fig. 7*B*, RIL was microinjected along the midline until rhythm cessation, which normally occurred within 7 min.

Respiratory period *in vitro* was computed from the average cycle time of 10 or more consecutive interinspiratory burst intervals, where each cycle was triggered by XII activity. We measured the amplitude and area of inspiratory drive potentials and XII motor output. The XII discharge was conditioned using a true RMS-to-DC converter (Analog Devices, One Technology Way, Norwood, MA, USA), which produces a full-wave rectified and smoothed XII waveform based on the root-mean-square of voltage input to the differential amplifier (Dagan Instruments, Minneapolis, MN, USA). The inspiratory drive potential was obtained by digitally filtering the intracellular voltage trajectory to remove spikes but preserve the amplitude and area of the underlying envelope of depolarization (e.g. Fig. 1*B* and *C*). The mean drive potential and XII motor output were obtained by averaging 10 consecutive respiratory cycles. The number of spikes was counted during 10 consecutive unfiltered inspiratory bursts. We compared these measures in control *versus* in the presence of various drugs using paired *t* tests, with significance for the two-tailed test at $P < 0.05$.

We recorded miniature EPSPs (mEPSPs) with 1 μM TTX to stop network activity and block I_{NaP}, and thus specifically measure the effects of RIL on the presynaptic probability of spontaneous neurotransmitter release. PTX (5 μM) and STR (5 μM) were applied to block inhibitory ionotropic receptors. A Cs^+-based patch solution was used to block K^+ currents and reduce electrotonic attenuation of synaptic potentials. Neurons were held at −60 mV using bias current. We generated a baseline noise histogram and a Gaussian distribution

was fitted to determine the standard deviation (S.D.) of baseline noise. Synaptic events were selected by a threshold-crossing algorithm with detection level to exceed 2 times the S.D., which makes the likelihood of detecting a spurious synaptic event $P < 0.05$. We tested whether RIL modified the amplitude or period of spontaneous mEPSPs using cumulative probability histograms and the Kolmogorov–Smirnov statistic (K-S test) with minimum probability at $P < 0.05$.

Results

PreBötC neurons exhibit inspiratory drive potentials with overriding spiking (Fig. 1*B*). Excitatory synaptic transmission initiates the inspiratory drive (Funk *et al.* 1993) and intrinsic currents with subthreshold activation like I_{NaP} are hypothesized to contribute to inspiratory drive potentials by amplifying synaptic depolarization (Butera *et al.* 1999*b*; Smith *et al.* 2000; Del Negro *et al.* 2001, 2002*a*).

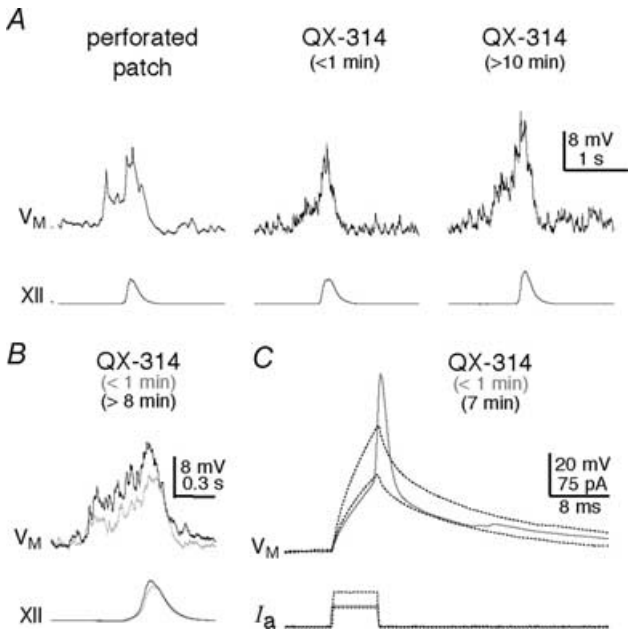

Figure 2. Measuring inspiratory drive potentials after attenuating Na^+ currents with QX-314
A, sequential experiment showing perforated patch, the first minute of whole cell, and the effects of QX-314 after more than 10 min of intracellular dialysis. *B*, superimposed traces from a different neuron showing the first minute of whole cell (grey) and the effects of QX-314 after more than 8 min (black). In both cases the inspiratory drive potential initiated 400 ms prior to XII discharge. *C*, within the first minute of whole-cell recording, action potentials could be evoked by depolarizing current pulses. However, after several minutes (e.g. 7 min shown) QX-314 blocked evoked action potentials. Even great increases in the depolarizing current pulses failed to evoke an active spike-like response. Baseline membrane potential was –60 mV.

Testing the role of Na^+ currents using intracellular QX-314

To measure the postsynaptic contribution of Na^+ currents in drive potential generation, we added 2 mM QX-314 to the potassium gluconate patch solution to block Na^+ currents intracellularly in only the recorded neuron while network properties and synaptic transmission remained unaltered. In contrast to higher doses, 2 mM QX-314 has minimal affects on Ca^{2+} currents (Talbot & Sayer, 1996; Hu *et al.* 2002), but still blocked action potential generation (Fig. 2*C*). Drive potentials in control were measured with perforated patch recording (Fig. 2*A*, left trace) and for one minute after rupturing the patch before QX-314 dialysed the cytosol (Fig. 2*A*, middle trace). After 8–10 min of whole-cell recording in the absence of Na^+ currents (e.g. Fig. 2*A*, right trace), both the amplitude and area of the drive potential increased to $140 \pm 13\%$ and $178 \pm 30\%$ of control, respectively ($P < 0.01$). In contrast, QX-314 had no effect on the onset latency, as determined by the appearance of synaptic potentials emerging from baseline noise prior to the inspiratory XII output ($P = 0.6$, $n = 6$, Fig. 2*B*). These findings suggest that the postsynaptic mechanisms involved in drive potentials remain undiminished, and in fact surprisingly increase following intracellular Na^+ channel blockade.

I_{NaP} promotes spiking during inspiratory bursts

QX-314 blocks all Na^+ currents, so it cannot be used to measure how I_{NaP} in particular contributes to drive potentials and regulates intraburst spike activity. We tested these roles of I_{NaP} with bath-applied 10 μM RIL, which blocks I_{NaP} within 6 min ($IC_{50} = 2.4$ μM) (Del Negro *et al.* 2002*b*; Ptak *et al.* 2005). While RIL may attenuate transient sodium currents (Do & Bean, 2003; Ptak *et al.* 2005), action potential generation is largely unaffected (Fig. 4*A* (inset) and Del Negro *et al.* 2002*b*).

However, RIL slowly depresses excitatory synaptic transmission (Doble, 1996; Wang *et al.* 2004). Therefore, we sought to establish a time window during which bath applications of RIL preferentially block I_{NaP} without perturbing synaptic transmission. In the presence of 1 μM TTX, 5 μM PTX and 5 μM STR, we recorded from inspiratory neurons using a Cs^+-based patch solution and measured the effects of bath-applied 10 μM RIL on spontaneous miniature EPSPs (mEPSPs; Fig. 3). In addition to silencing the network, TTX also precluded the effects of RIL on I_{NaP}, and thus isolated the effects of RIL on transmission. In the first 6–8 min, RIL had no effect on mEPSPs; there was no significant displacement of the cumulative amplitude histogram (Fig. 3*B*) or the cumulative period histogram ($P > 0.05$, $n = 4$, Fig. 3*C*).

After 12 min, RIL exposure significantly decreased mEPSP frequency, as shown by a significant rightward

shift in the cumulative period histogram ($P < 0.05$, Fig. 3*C*), without significant effects on the cumulative amplitude histogram ($P > 0.05$, Fig. 3*B*). Thus, 10 μM RIL (12–14 min) attenuated the probability of quantal neurotransmitter release, which is consistent with inhibitory effects on presynaptic neurotransmission, and due to the experimental conditions, this effect cannot be attributed to reduction of I_{NaP}.

In rhythmically active slices, 10 μM RIL exposure for 6–8 min significantly reduced the number of spikes per burst to $58 \pm 10\%$ of control (from 6.1 ± 1.3 to 3.9 ± 1.3, $P < 0.01$) but had no effect on inspiratory drive potentials: amplitude and area remained at $103 \pm 5\%$ and $96 \pm 6\%$ of control ($P > 0.4$). XII amplitude and area were also unaffected: $102 \pm 4\%$ and $103 \pm 6\%$ of control, respectively (both $P > 0.5$). Respiratory frequency remained at $87 \pm 9\%$ of control ($P = 0.3$, $n = 4$, Fig. 4*A*).

However, after 15 min (at which time RIL caused presynaptic inhibition, e.g. Fig. 3), 10 μM RIL decreased the amplitude and area of drive potentials to $62 \pm 8\%$ and $41 \pm 9\%$ of control and further reduced the intraburst spiking to $22 \pm 8\%$ of control (all $P < 0.05$). XII amplitude and area both decreased significantly to $63 \pm 7\%$ of control, and respiratory frequency decreased to $60 \pm 18\%$ of control (all $P < 0.05$, $n = 4$, Fig. 4*A*).

We used a low concentration of TTX (20 nM) as an alternative agent to evaluate the role of I_{NaP}. Figure 4*C* shows the steady-state current–voltage (*I–V*) relation after blocking synaptic transmission and Ca^{2+} channels with a low Ca^{2+} ACSF containing 200 μM Cd^{2+}. TTX (20 nM) selectively reduced the inwardly rectifying or negative slope region of the *I–V* curve within 4–6 min ($n = 5$, Fig. 4*C* and *D*). The TTX-sensitive inward current (measured at steady-state during 500 ms-long voltage steps) activated near −60 mV and peaked near −40 mV, indicative of I_{NaP} in respiratory neurons (Del Negro *et al.* 2002*a*; Rybak *et al.* 2003; Ptak *et al.* 2005). Subsequently adding 1 μM TTX to the bath solution caused little additional attenuation ($n = 3$, Fig. 4*C* and *D*) suggesting that I_{NaP} is quickly and effectively blocked by 20 nM TTX.

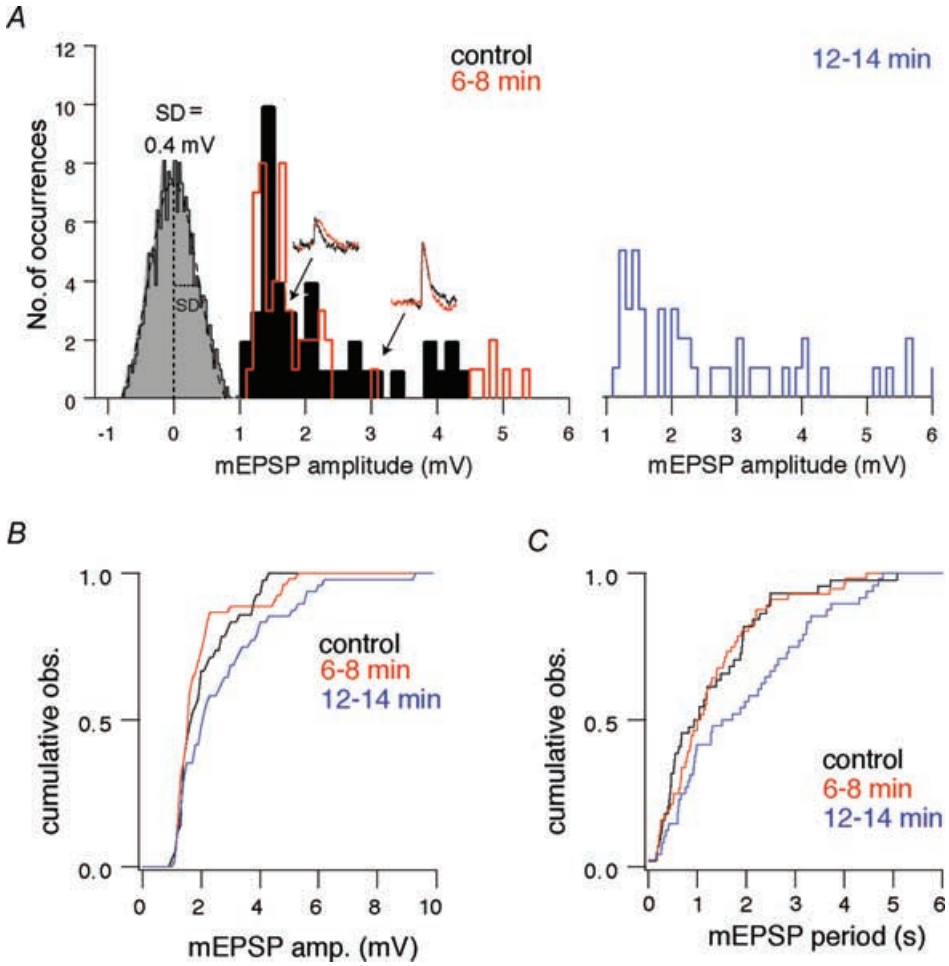

Figure 3. The effects of 10 μM RIL on mEPSPs
A, amplitude histograms for control (black) in the presence of riluzole (RIL) for 6–8 min (red) and 12–14 min (blue). Inset traces show sample mEPSPs for control and RIL conditions. A histogram of baseline noise is also shown, with S.D. = 0.4 mV. *B*, cumulative mEPSP amplitude histogram. *C*, cumulative mEPSP period histogram.

Next, we tested the effects of 20 nM TTX on inspiratory drive potential generation. TTX significantly decreased the number of spikes per burst to 44 ± 8% of control within 4–8 min (from 17.8 ± 3.5 to 8.0 ± 2.5, $P < 0.05$) but did not affect the amplitude or area of drive potentials, which remained at 100 ± 6% and 94 ± 9% of control, respectively (both $P > 0.6$). Within 4–8 min, 20 nM TTX had no effect on XII motor output or respiratory frequency (all $P > 0.2$, $n = 5$, Fig. 4*B*). However, after 10–40 min of exposure, 20 nM TTX suppressed spiking activity and ultimately led to rhythm cessation (Del Negro *et al.* 2005).

Microinjection experiments to test whether I_{NaP} and pacemakers are obligatory

To limit the effects of RIL and TTX on respiratory-related neurons situated outside the preBötC, we performed bilateral microinjection experiments that target drug delivery within the preBötC. To verify that our microinjection pipettes were accurately positioned, we first bilaterally microinjected the $GABA_A$ receptor agonist muscimol (MUS, 15 μM), which when properly placed stopped the rhythm within 20–60 s. Moving either pipette 90–150 μm from the optimal position failed to block rhythmogenesis, even after 10 min of continuous microinjection ($n = 3$, Fig. 5).

In every experiment, we first used the control MUS injection protocol (Fig. 5) to verify the correct positioning of the microinjection pipettes. After recovery from MUS, we bilaterally microinjected 10 μM RIL for > 20 min, which had no effect on the amplitude (94 ± 5% of control, $P > 0.25$), area (90 ± 6% of control, $P > 0.09$) or period of XII motor output (94 ± 5% of control, $P > 0.25$). RIL in the preBötC did not destabilize the rhythm; the coefficient of variation (CV) of the period was 0.22 ± 0.03 in control *versus* 0.21 ± 0.01 during 10 μM RIL microinjection ($P = 0.6$, $n = 5$, Fig. 6*A*).

We employed slices within a developmental period (P0–4) containing exceedingly few, if any, pacemaker neurons that depend on I_{CAN} (Pena *et al.* 2004; Del Negro *et al.* 2005). To rule out the unlikely rhythmogenic contribution of I_{CAN} pacemaker neurons, we added 100 μM FFA to the bath solution during bilateral RIL microinjection. FFA was applied for > 20 min;

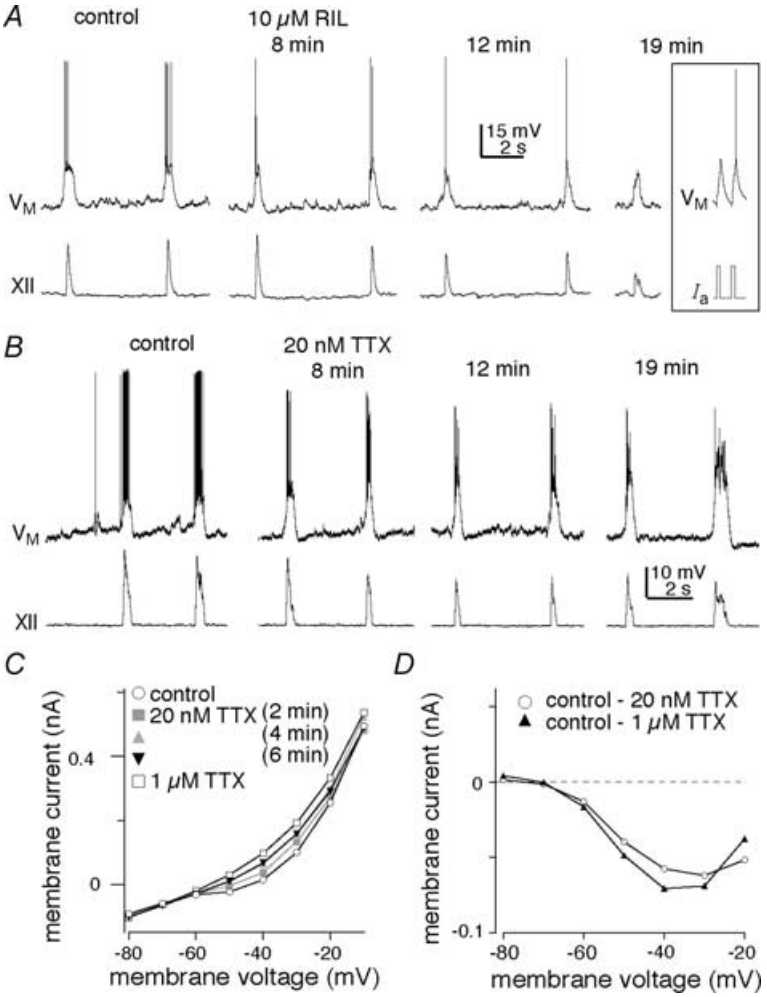

Figure 4. The role of I_{NaP} in inspiratory drive potentials
A and *B*, sample traces of two consecutive inspiratory cycles are shown for control and 10 μM RIL (*A*) and 20 nM TTX (*B*) at 8, 12 and 19 min. Inset in *A* shows spikes evoked by 5 ms current pulses to show that RIL did not attenuate action potentials even after > 20 min of exposure. *A* and *B* have separate scale bars. Baseline membrane potential was –60 mV. *C*, steady-state *I–V* curve measured in the presence of low Ca^{2+} solution and 200 μM Cd^{2+} showing control (open circles) and the blockade of inward rectification due to I_{NaP} by 20 nM TTX at membrane potentials greater than –60 mV. Conditions with 20 nM TTX are shown at 2 min (grey boxes), 4 min (grey triangles), and 6 min (black inverted triangles). Note: 4 and 6 min trials overlie one another and thus indicate 20 nM TTX effects at steady state. The subsequent application of 1 μM TTX (open squares) caused some additional attenuation of the inward rectification above –60 mV. *D*, TTX-sensitive subtracted currents: the 20 nM TTX (6 min) *I–V* curve was subtracted from the control *I–V* curve to reveal the 20 nM TTX-sensitive current (open circles). The 1 μM TTX-sensitive current (black triangles) was obtained by subtracting the 1 μM TTX *I–V* curve from control.

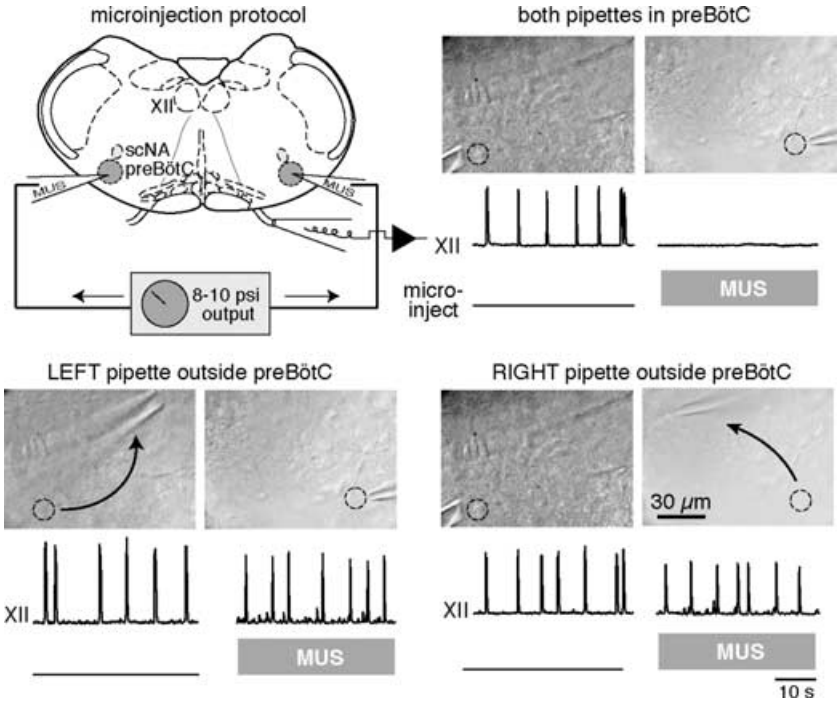

Figure 5. Bilateral microinjection of 15 μM MUS in the preBötC
Schematic representation of the slice preparation showing microinjection pipettes. Below each photograph of microinjection pipettes the XII trace shows respiratory motor output *in vitro* and the 'microinject' trace reflects transistor–transistor logic (TTL) pulses at 3 Hz that gate the micropressure drug-delivery injections. Bilateral microinjection of MUS stops the XII rhythm within 1 min, whereas microinjection of MUS unilaterally in the preBötC does not cause rhythm cessation; microinjection pipettes were moved one at a time 90–150 μm. All traces depict the last 40 s of data acquired in each pharmacological condition. Circles mark the effective location for microinjection pipettes. Time calibration is shown.

the cumulative RIL microinjection time was >40 min. Together, FFA and RIL significantly reduced the amplitude and area of the XII motor output to $82 \pm 4\%$ and $63 \pm 5\%$ of control, respectively (both $P < 0.05$), but had no significant effect on respiratory period ($120 \pm 11\%$ of control, $P > 0.25$) or CV (0.19 ± 0.06, $P > 0.25$, $n = 5$, Fig. 6*A*).

Unlike local application in the preBötC, e.g. Fig. 6*A*, bath application of 10 μM RIL in conjunction with 100 μM FFA stops rhythmogenesis *in vitro* (Pena *et al.* 2004; Del Negro

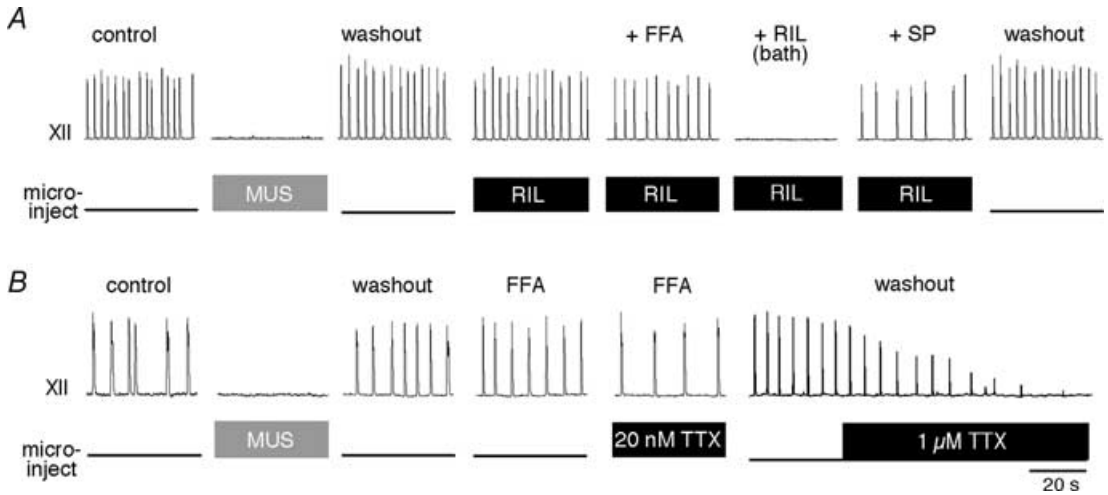

Figure 6. Sequential drug application experiments using local microinjection of 10 μM RIL or 20 nM TTX
Top traces show XII motor output, lower traces labelled 'microinject' reflect TTL pulses at 3 Hz that gate micropressure drug-delivery injections. *A*, bilateral injection of 15 μM MUS was used to verify the position of the microinjection pipettes, identical to Fig. 5. After recovering the rhythm, 10 μM RIL was microinjected for >20 min, followed by bath application of 100 μM flufenamic acid (FFA). After >20 min of bath-applied FFA (cumulative RIL exposure >40 min), we added 10 μM RIL to the bath, which stopped the rhythm within 7 min. Finally 0.5 μM substance P (SP) was added to revive rhythmic activity. Recovery from all drugs occurred within 1–2 h and is shown as washout. *B*, bilateral injection of 15 μM MUS was used to verify the position of the microinjection pipettes (as in *A* and Fig. 5). After recovering the rhythm, we added 100 μM FFA for >15 min and then microinjected 20 nM TTX for >10 min. All traces depict the last 40 s of data acquired in each pharmacological condition. Time calibration in *B* applies to both experiments.

et al. 2005). We replicated this result in the microinjection experiment by subsequently bath-applying 10 μM RIL with 100 μM FFA, in which case the rhythm stopped in 7.4 ± 2.2 min ($n = 5$). After ≥ 2 min of rhythm cessation, we applied 0.5 μM substance P (SP), which revived respiratory rhythm in 3 of 5 slices. This suggests that bath application of RIL affects the state of neuronal excitability in the preBötC, but does not cause a fundamental breakdown in the rhythmogenic mechanisms since SP can recover the rhythm in the majority of slices tested. In all cases, XII motor output recovered in washout of > 1.5 h ($n = 5$, Fig. 6*A*).

We repeated the experiment in Fig. 6*A* using 20 nM TTX instead of RIL. To preclude any possible contribution due to I_{CAN} pacemaker neurons, we bath-applied 100 μM FFA for > 15 min before bilaterally microinjecting 20 nM TTX directly into the preBötC for > 10 min. TTX microinjection in the presence of FFA had no significant effect on the amplitude and area of XII motor output ($P > 0.4$, $n = 4$). Respiratory period increased to $133 \pm 9\%$ compared to the control following recovery from MUS ($P < 0.05$, $n = 4$), but did not stop after > 10 min of TTX bilateral microinjection in the presence of FFA. After washout from local 20 nM TTX, we microinjected 1 μM TTX directly into the preBötC, which caused rhythm cessation within 1 min and verified the ability of TTX to quickly penetrate the tissue ($n = 2$, Fig. 6*B*).

Microinjection experiments outside the preBötC to test the rhythm-generating role of I_{NaP} in neurons outside the preBötC

In the presence of bath-applied FFA, bath-applied RIL caused rhythm cessation whereas local RIL application within the preBötC did not. To explain these observations, we hypothesized that I_{NaP} in areas outside the preBötC is important for maintaining rhythmogenesis. One possible target is serotonergic neurons in the raphe, which help maintain preBötC neuron excitability. We tested whether blocking I_{NaP} in the raphe region would decrease excitability in the preBötC to perturb or prevent rhythmogenesis. We locally microinjected 10 μM RIL along the midline in the raphe obscurus in the presence of 100 μM FFA; XII motor output stopped in 3–6 min ($n = 6$, Fig. 7). In all cases, XII motor output recovered fully in washout.

Discussion

The discovery of bursting neurons in the preBötC (Smith *et al.* 1991) sparked great interest in the rhythmogenic role of I_{NaP} in respiration and led to the hypothesis that I_{NaP} amplifies excitatory synaptic drive and promotes inspiratory bursts throughout the network. However, due to the unspecific nature of I_{NaP} pharmacology, evaluating the obligatory role of I_{NaP} is problematic. Since the same subtypes of Na^+ channels underlie both transient and persistent modes of gating (Taddese & Bean, 2002; Do & Bean, 2003; Ptak *et al.* 2005), I_{NaP} antagonists, like RIL and low concentrations of TTX, also attenuate transient Na^+ currents in preBötC neurons (Del Negro *et al.* 2005; Ptak *et al.* 2005). Additionally, RIL affects Ca^{2+} channels, Ca^{2+}-dependent K^+ channels, $GABA_A$ receptors and leads to the general depression of excitatory neurotransmission (Fig. 3 and Doble, 1996; Huang *et al.* 1997; Wu & Li, 1999; He *et al.* 2002; Wang *et al.* 2004). Furthermore, I_{NaP} is expressed by all preBötC neurons, including the majority that are without pacemaker properties (Del Negro *et al.* 2002*a*), and in several other types of medullary neurons (Umemiya & Berger, 1995; Rybak *et al.* 2003; Ptak *et al.* 2005; Zeng *et al.* 2005). Recognizing these pharmacological limitations, we systematically tested the role of I_{NaP} in preBötC neurons by using various pharmacological agents and protocols, which all yielded consistent results.

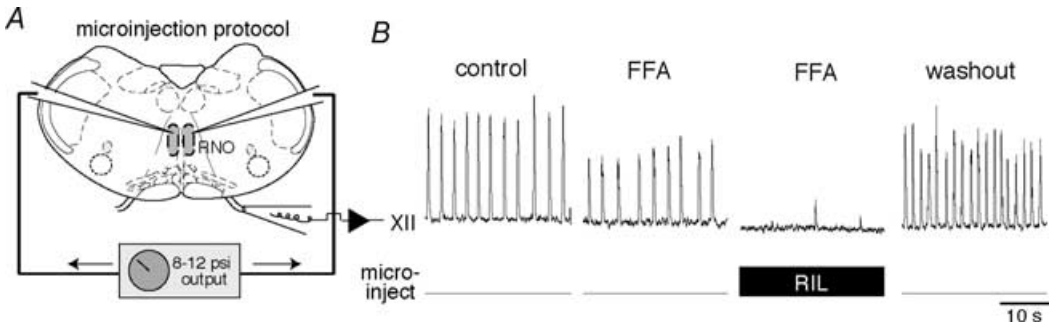

Figure 7. Bilateral microinjection of 10 μM RIL into midline raphe
A, schematic representation of the slice preparation showing microinjection pipettes positioned in the raphe nucleus obscurus (RNO). Top traces show XII motor output, lower traces labelled 'microinject' reflect TTL pulses at 3 Hz that gate micropressure drug-delivery injections. *B*, 100 μM FFA was applied to the bath for > 15 min. Subsequent microinjection of 10 μM RIL to the RNO caused rhythm cessation (trace taken at 6.5 min). The XII motor output fully recovered in washout (trace shown after 1 h). All traces were taken at the end of the respective pharmacological condition.

We first analysed whether transient and persistent Na^+ currents contribute to synaptic amplification by blocking their actions using intracellular application of QX-314 and found that inspiratory drive potentials actually increased. The inability of 20 nM TTX and RIL to attenuate drive potentials within 8 min of drug application supports the notion that I_{NaP} does not contribute to drive potential generation. Both drugs blocked I_{NaP} within 6 min of drug application (Fig. 4*C* and Del Negro *et al.* 2005). While we applied both TTX and RIL for > 19 min, after 12 min these agents perturbed other cellular and network properties that are important in rhythmogenesis (see above). That QX-314 caused a statistically significant increase in the drive potential may reflect the removal of a Na^+ channel-mediated shunt, but this remains to be tested.

In contrast, we found that blocking I_{NaP} with either 10 μM RIL or 20 nM TTX decreased the number of spikes per burst by 40–50%, suggesting that I_{NaP} promotes intraburst spike output. This is consistent with the expression of I_{NaP} predominantly at the soma and axon initial segment where it assists in spike initiation and promotes repetitive firing (Lee & Heckman, 2001; Astman *et al.* 2006; Palmer & Stuart, 2006) and in proximal dendrites (Mittmann *et al.* 1997). Additionally, I_{NaP} is measurable in acutely dissociated respiratory neurons that are extensively denuded of dendritic processes (Ptak *et al.* 2005), which confirms I_{NaP} expression in the soma/axon initial segment of preBötC neurons.

To explore the rhythmogenic role of I_{NaP} in preBötC neurons, we used microinjection protocols to deliver drugs directly into the preBötC. Putatively rhythmogenic preBötC neurons are interneurons (Gray *et al.* 1999) that form synapses onto somata and dendrites within the preBötC (Guyenet & Wang, 2001; Wang *et al.* 2001; Stornetta *et al.* 2003). The extent to which I_{NaP} is expressed in preBötC neuron dendrites is presently unknown. However, drugs microinjected directly into the preBötC will affect I_{NaP} at both somatic and dendritic sites contained within the preBötC.

The fact that RIL and TTX did not stop the rhythm when microinjected in the preBötC in the presence of 100 μM FFA indicates that I_{NaP} and associated pacemaker properties are nonessential for rhythmogenesis. Since RIL was applied directly within the preBötC, its low solubility (Doble, 1996) was not a factor that would prevent RIL from penetrating the rhythm-generating network. This fact is underscored by identical microinjection protocols in the raphe that did stop the rhythm within 6 min, confirming that RIL did affect the neurons at the injection site.

In contrast to RIL, TTX reduced the frequency of XII motor output in the presence of 100 μM FFA. This reduction in frequency is most likely attributable to the attenuation of spike-generating currents caused by 20 nM TTX after several minutes of exposure (Fig. 4*B*, 19 min; and Del Negro *et al.* 2005). Despite these additional effects, 20 nM TTX ultimately failed to block rhythmogenesis. Changing the concentration of microinjected TTX from 20 nM to 1 μM quickly caused rhythm cessation and confirmed that TTX rapidly affected preBötC neurons.

The fact that RIL and TTX reduced intraburst spiking by ~50% without affecting drive potentials appears paradoxical. In a highly interconnected network, such as in the preBötC (Rekling *et al.* 2000), reductions in neuronal firing would be expected to diminish the presynaptic neurotransmitter release underlying postsynaptic drive potential generation, and thus reduce the magnitude of the drive potential. However, intrinsic burst-generating currents that are activated by synaptic input could compensate for significant reductions in presynaptic transmitter release, as long as postsynaptic activity is sufficient to activate these currents. The I_{NaP}-independent ionic mechanisms for synaptic amplification, and their activation mechanisms, remain to be determined.

In its generalized form, the *pacemaker hypothesis* posits that pacemaker neurons are obligatory for rhythmogenesis (Smith *et al.* 1991). More recently, the hypothesis that either I_{NaP}- or I_{CAN}-mediated pacemakers can drive the rhythm independently has been proposed (Ramirez *et al.* 2004). Accordingly, to stop rhythm generation both pacemaker phenotypes must be blocked.

The *hybrid pacemaker-network* version of the pacemaker hypothesis (Smith *et al.* 1991, 2000) is founded on an essential core population of I_{NaP} pacemaker neurons but the role of I_{NaP} extends to non-pacemaker neurons where it is postulated to amplify excitatory synaptic drive and enhance inspiratory burst generation. Accordingly, the dynamic interactions of non-pacemaker and pacemaker neurons control respiratory frequency (Butera *et al.* 1999*a*, 2000; Best *et al.* 2005).

Our results are not consistent with either the generalized or hybrid versions of the pacemaker hypothesis. First, I_{NaP} did not amplify synaptic excitation *per se* but did enhance production of action potentials. Second, the rhythm continued in the presence of I_{CAN} and I_{NaP} antagonists (Fig. 6), which stop all known pacemaker-neuron activity (Del Negro *et al.* 2002*b*, 2005; Pena *et al.* 2004). The observation that bath application of both I_{NaP} and I_{CAN} antagonists can stop respiratory rhythmogenesis *in vitro* has been used to support the generalized pacemaker hypothesis (Pena *et al.* 2004; Paton *et al.* 2006; Tryba *et al.* 2006). However, this interpretation is flawed for the following reasons. (i) The rhythm can be revived with either SP or AMPA (see Fig. 6*A* and Del Negro *et al.* 2005; Feldman & Del Negro, 2006). This indicates that the fundamental mechanism of rhythmogenesis was intact after pharmacological elimination of pacemaker properties; all that was required was a sufficient boost in excitability via exogenous agents. (ii) Bath application

of drugs affects all neurons within the slice preparation, including key populations external to the preBötC such as raphe neurons, respiratory premotoneurons and XII motoneurons. The effects of these antagonists on other populations of respiratory-related neurons can readily explain their effects on rhythm without the need to invoke any changes in preBötC neuron function.

For example, blocking I_{NaP} in raphe obscurus neurons in the presence of 100 μM FFA caused rhythm cessation. The raphe neurons project to and appear to increase neuronal excitability in the preBötC (Di Pasquale *et al.* 1994; Al-Zubaidy *et al.* 1996; Bou-Flores *et al.* 2000; Pena & Ramirez, 2002). This experiment can potentially explain why, in the presence of FFA, blocking I_{NaP} with RIL locally applied to the preBötC had no effect on respiratory frequency, whereas the subsequent addition of RIL to the bath stopped the rhythm within 7 min (a timeframe that indicates RIL was still primarily acting on I_{NaP}). We propose that I_{NaP} in raphe, and possibly other respiratory-related neurons exclusive of the preBötC can influence excitability within the rhythmogenic network.

Our study illustrates that data obtained following bath-application of drugs to slices must be cautiously interpreted and need multiple controls. In particular, the network level effects of bath-applied drugs cannot be casually attributed to a small subpopulation of preBötC pacemaker neurons embedded in active slices that contain numerous respiratory interneurons as well as premotor and motoneurons.

Pacemaker neurons with as yet undiscovered biophysical mechanisms, i.e. neither I_{NaP} nor I_{CAN}, for bursting may play a role generating respiratory rhythm, but the existence of such neurons remains to be demonstrated. Otherwise, the accumulating evidence suggests that pacemaker neurons are not obligatory for respiratory rhythm generation (Del Negro *et al.* 2002*b*, 2005; Kosmidis *et al.* 2004). Instead, we suggest the *group-pacemaker hypothesis* (Rekling & Feldman, 1998; Feldman & Del Negro, 2006) as a viable alternative explanation. In this framework, periodic inspiratory bursts result from recurrent excitatory connections within the preBötC. Intrinsic currents will naturally play a role in recurrent excitation. We postulate that an inward current that can be directly evoked synaptically via intracellular signalling would be advantageous in this regard compared to a voltage-dependent current like I_{NaP}, because its burst-generating function need not depend on the baseline membrane potential. In contrast, I_{NaP} only influences respiratory neurons in a voltage window between −60 and −40 mV: I_{NaP} remains in a deactivated state when the membrane potential is too low and its contribution steadily diminishes at depolarized potentials due to steady-state inactivation (Butera *et al.* 1999*a*; Del Negro *et al.* 2001, 2002*a*; Ptak *et al.* 2005). The activation properties of an inward current directly coupled to synaptic input need not be subject to voltage fluctuations and would therefore be well equipped to amplify synaptic excitation and promote robust and reliable inspiratory bursts.

References

Al-Zubaidy ZA, Erickson RL & Greer JJ (1996). Serotonergic and noradrenergic effects on respiratory neural discharge in the medullary slice preparation of neonatal rats. *Pflugers Arch* **431**, 942–949.

Astman N, Gutnick MJ & Fleidervish IA (2006). Persistent sodium current in layer 5 neocortical neurons is primarily generated in the proximal axon. *J Neurosci* **26**, 3465–3473.

Best J, Borisyuk A, Rubin J, Terman D & Wechselberger M (2005). The dynamic range of bursting in a model of respiratory pacemaker network. *SIAM J Appl Dyn Syst* **4**, 1007–1139.

Bou-Flores C, Lajard AM, Monteau R, De Maeyer E, Seif I, Lanoir J & Hilaire G (2000). Abnormal phrenic motoneuron activity and morphology in neonatal monoamine oxidase A-deficient transgenic mice: possible role of a serotonin excess. *J Neurosci* **20**, 4646–4656.

Brockhaus J & Ballanyi K (1998). Synaptic inhibition in the isolated respiratory network of neonatal rats. *Eur J Neurosci* **10**, 3823–3839.

Butera RJ, Johnson SM, Del Negro CA, Rinzel J & Smith JC (2000). Dynamics of excitatory networks of pacemaker neurons: experimental and modeling studies of the respiratory rhythm generator. In *Neurocomputing*, ed. Bower J, pp. 323–330. Elsevier, Amsterdam.

Butera RJ Jr, Rinzel J & Smith JC (1999*a*). Models of respiratory rhythm generation in the pre-Bötzinger complex. I. Bursting pacemaker neurons. *J Neurophysiol* **82**, 382–397.

Butera RJ Jr, Rinzel J & Smith JC (1999*b*). Models of respiratory rhythm generation in the pre-Bötzinger complex. II. Populations of coupled pacemaker neurons. *J Neurophysiol* **82**, 398–415.

Butera RJ, Rubin J, Terman D & Smith JC (2005). Oscillatory bursting mechanisms in respiratory pacemaker neurons and networks. In *Bursting the Genesis of Rhythm in the Nervous System*, ed.Coombes S & Bressloff PC. World Scientific Publishing, New Jersey.

Del Negro CA, Johnson SM, Butera RJ & Smith JC (2001). Models of respiratory rhythm generation in the pre-Bötzinger complex. III. Experimental tests of model predictions. *J Neurophysiol* **86**, 59–74.

Del Negro CA, Koshiya N, Butera RJ Jr & Smith JC (2002*a*). Persistent sodium current, membrane properties and bursting behavior of pre-Bötzinger complex inspiratory neurons in vitro. *J Neurophysiol* **88**, 2242–2250.

Del Negro CA, Morgado-Valle C & Feldman JL (2002*b*). Respiratory rhythm: an emergent network property? *Neuron* **34**, 821–830.

Del Negro CA, Morgado-Valle C, Hayes JA, Mackay DD, Pace RW, Crowder EA & Feldman JL (2005). Sodium and calcium dependent pacemaker neurons and respiratory rhythm generation. *J Neurosci* **25**, 446–453.

Di Pasquale E, Monteau R & Hilaire G (1994). Endogenous serotonin modulates the fetal respiratory rhythm: an in vitro study in the rat. *Brain Res Dev Brain Res* **80**, 222–232.

Do MT & Bean BP (2003). Subthreshold sodium currents and pacemaking of subthalamic neurons: modulation by slow inactivation. *Neuron* **39**, 109–120.

Doble A (1996). The pharmacology and mechanism of action of riluzole. *Neurology* **47**, S233–S241.

Feldman JL & Del Negro CA (2006). Looking for inspiration: new perspectives on respiratory rhythm. *Nat Rev Neurosci* **7**, 232–241.

Feldman JL & Smith JC (1989). Cellular mechanisms underlying modulation of breathing pattern in mammals. *Ann N Y Acad Sci* **563**, 114–130.

Funk GD, Smith JC & Feldman JL (1993). Generation and transmission of respiratory oscillations in medullary slices: role of excitatory amino acids. *J Neurophysiol* **70**, 1497–1515.

Gray PA, Rekling JC, Bocchiaro CM & Feldman JL (1999). Modulation of respiratory frequency by peptidergic input to rhythmogenic neurons in the preBötzinger complex. *Science* **286**, 1566–1568.

Guyenet PG & Wang H (2001). Pre-Bötzinger neurons with preinspiratory discharges 'in vivo' express NK1 receptors in the rat. *J Neurophysiol* **86**, 438–446.

He Y, Benz A, Fu T, Wang M, Covey DF, Zorumski CF & Mennerick S (2002). Neuroprotective agent riluzole potentiates postsynaptic $GABA_A$ receptor function. *Neuropharmacology* **42**, 199–209.

Hu GY, Biro Z, Hill RH & Grillner S (2002). Intracellular QX-314 causes depression of membrane potential oscillations in lamprey spinal neurons during fictive locomotion. *J Neurophysiol* **87**, 2676–2683.

Huang CS, Song JH, Nagata K, Yeh JZ & Narahashi T (1997). Effects of the neuroprotective agent riluzole on the high voltage-activated calcium channels of rat dorsal root ganglion neurons. *J Pharmacol Exp Ther* **282**, 1280–1290.

Johnson SM, Smith JC, Funk GD & Feldman JL (1994). Pacemaker behavior of respiratory neurons in medullary slices from neonatal rat. *J Neurophysiol* **72**, 2598–2608.

Kosmidis EK, Pierrefiche O & Vibert JF (2004). Respiratory-like rhythmic activity can be produced by an excitatory network of non-pacemaker neuron models. *J Neurophysiol* **92**, 686–699.

Lee RH & Heckman CJ (2001). Essential role of a fast persistent inward current in action potential initiation and control of rhythmic firing. *J Neurophysiol* **85**, 472–475.

Mittmann T, Linton SM, Schwindt P & Crill W (1997). Evidence for persistent Na^+ current in apical dendrites of rat neocortical neurons from imaging of Na^+-sensitive dye. *J Neurophysiol* **78**, 1188–1192.

Onimaru H, Arata A & Homma I (1995). Intrinsic burst generation of preinspiratory neurons in the medulla of brainstem-spinal cord preparations isolated from newborn rats. *Exp Brain Res* **106**, 57–68.

Palmer LM & Stuart GJ (2006). Site of action potential initiation in layer 5 pyramidal neurons. *J Neurosci* **26**, 1854–1863.

Paterson DS, Trachtenberg FL, Thompson EG, Belliveau RA, Beggs AH, Darnall R, Chadwick AE, Krous HF & Kinney HC (2006). Multiple serotonergic brainstem abnormalities in sudden infant death syndrome. *JAMA* **296**, 2124–2132.

Paton JF (1996). The ventral medullary respiratory network of the mature mouse studied in a working heart–brainstem preparation. *J Physiol* **493**, 819–831.

Paton JF, Abdala AP, Koizumi H, Smith JC & St-John WM (2006). Respiratory rhythm generation during gasping depends on persistent sodium current. *Nat Neurosci* **9**, 311–313.

Pena F, Parkis MA, Tryba AK & Ramirez JM (2004). Differential contribution of pacemaker properties to the generation of respiratory rhythms during normoxia and hypoxia. *Neuron* **43**, 105–117.

Pena F & Ramirez JM (2002). Endogenous activation of serotonin-2A receptors is required for respiratory rhythm generation in vitro. *J Neurosci* **22**, 11055–11064.

Ptak K, Zummo GG, Alheid GF, Tkatch T, Surmeier DJ & McCrimmon DR (2005). Sodium currents in medullary neurons isolated from the pre-Bötzinger complex region. *J Neurosci* **25**, 5159–5170.

Ramirez JM, Tryba AK & Pena F (2004). Pacemaker neurons and neuronal networks: an integrative view. *Curr Opin Neurobiol* **14**, 665–674.

Rekling JC & Feldman JL (1998). PreBötzinger complex and pacemaker neurons: hypothesized site and kernel for respiratory rhythm generation. *Annu Rev Physiol* **60**, 385–405.

Rekling JC, Shao XM & Feldman JL (2000). Electrical coupling and excitatory synaptic transmission between rhythmogenic respiratory neurons in the preBötzinger complex. *J Neurosci* **20**, RC113.

Ruangkittisakul A, Schwarzacher SW, Secchia L, Poon BY, Ma Y, Funk GD & Ballanyi K (2006). High sensitivity to neuromodulator-activated signaling pathways at physiological $[K^+]$ of confocally imaged respiratory center neurons in on-line-calibrated newborn rat brainstem slices. *J Neurosci* **26**, 11870–11880.

Rybak IA, Ptak K, Shevtsova NA & McCrimmon DR (2003). Sodium currents in neurons from the rostroventrolateral medulla of the rat. *J Neurophysiol* **90**, 1635–1642.

Smith JC, Butera RJ, Koshiya N, Del Negro C, Wilson CG & Johnson SM (2000). Respiratory rhythm generation in neonatal and adult mammals: the hybrid pacemaker-network model. *Respir Physiol* **122**, 131–147.

Smith JC, Ellenberger HH, Ballanyi K, Richter DW & Feldman JL (1991). Pre-Bötzinger complex: a brainstem region that may generate respiratory rhythm in mammals. *Science* **254**, 726–729.

Smith JC, Greer JJ, Liu GS & Feldman JL (1990). Neural mechanisms generating respiratory pattern in mammalian brain stem-spinal cord in vitro. I. Spatiotemporal patterns of motor and medullary neuron activity. *J Neurophysiol* **64**, 1149–1169.

Stornetta RL, Rosin DL, Wang H, Sevigny CP, Weston MC & Guyenet PG (2003). A group of glutamatergic interneurons expressing high levels of both neurokinin-1 receptors and somatostatin identifies the region of the pre-Bötzinger complex. *J Comp Neurol* **455**, 499–512.

Suzue T (1984). Respiratory rhythm generation in the *in vitro* brain stem–spinal cord preparation of the neonatal rat. *J Physiol* **354**, 173–183.

Taddese A & Bean BP (2002). Subthreshold sodium current from rapidly inactivating sodium channels drives spontaneous firing of tuberomammillary neurons. *Neuron* **33**, 587–600.

Talbot MJ & Sayer RJ (1996). Intracellular QX-314 inhibits calcium currents in hippocampal CA1 pyramidal neurons. *J Neurophysiol* **76**, 2120–2124.

Thoby-Brisson M & Ramirez JM (2001). Identification of two types of inspiratory pacemaker neurons in the isolated respiratory neural network of mice. *J Neurophysiol* **86**, 104–112.

Tryba AK, Pena F & Ramirez JM (2006). Gasping activity in vitro: a rhythm dependent on 5-HT2A receptors. *J Neurosci* **26**, 2623–2634.

Umemiya M & Berger AJ (1995). Inhibition by riluzole of glycinergic postsynaptic currents in rat hypoglossal motoneurones. *Br J Pharmacol* **116**, 3227–3230.

Wang H, Stornetta RL, Rosin DL & Guyenet PG (2001). Neurokinin-1 receptor-immunoreactive neurons of the ventral respiratory group in the rat. *J Comp Neurol* **434**, 128–146.

Wang SJ, Wang KY & Wang WC (2004). Mechanisms underlying the riluzole inhibition of glutamate release from rat cerebral cortex nerve terminals (synaptosomes). *Neuroscience* **125**, 191–201.

Wu SN & Li HF (1999). Characterization of riluzole-induced stimulation of large-conductance calcium-activated potassium channels in rat pituitary GH3 cells. *J Invest Med* **47**, 484–495.

Zeng J, Powers RK, Newkirk G, Yonkers M & Binder MD (2005). Contribution of persistent sodium currents to spike-frequency adaptation in rat hypoglossal motoneurons. *J Neurophysiol* **93**, 1035–1041.

Acknowledgements

This work was supported by the National Science Foundation (USA; IOB-0616099), National Institutes of Health (USA; HL-40959), the Jeffress Memorial Trust (Richmond, Virginia, USA), and the Suzann Wilson Matthews Faculty Research Award (The College of William and Mary, Williamsburg, Virginia, USA).